4-2007

Behaviour of reinforced self-consolidating concrete frames

Aly Said
University of Nevada - Las Vegas, aly.said@unlv.edu

Moncef Nehdi
University of West Ontario, Canada

Proceedings of the Institution of Civil Engineers
Structures & Buildings 160
April 2007 Issue SB2
Pages 95–104

Paper 14291
Received 17/05/2005
Accepted 13/12/2006

Keywords:
concrete structures/seismic engineering

Aly Said
Assistant Professor, University of Nevada, Las Vegas, USA

Moncef Nehdi
Associate Professor, University of West Ontario, Canada

ice
Institution of Civil Engineers

Behaviour of reinforced self-consolidating concrete frames

A. Said PhD and M. Nehdi PhD, PEng

Multi-storey reinforced concrete (RC) structural frames represent some of the most congested structural elements. Placing and consolidating concrete in such structural frames imposes substantial challenges. This offers a unique area of application for self-consolidating concrete (SCC) because of its inherent ability to flow under its own weight and fill congested sections, complicated formwork and hard-to-reach areas. Research is, however, needed to demonstrate the ability of SCC structural frames adequately to resist vertical and lateral loads. In the present study, full-scale 3 m high beam-column joints reinforced as per the Canadian Standards CSA A23·3-94 and ACI-352R-02 were made with normal concrete (NC) and SCC. They were tested under reversed cyclic loading applied at the beam tip and at a constant axial load applied on the column. The beam–column joint specimens were instrumented with linear variable displacement transducers and strain gauges to determine load–displacement traces, cumulative dissipated energy and secant stiffness. The current paper compares the performance of reinforced NC and SCC structural frames and discusses the potential use of SCC in such structural elements. Results indicate that reducing the coarse aggregate content in SCC mixtures can reduce the contribution of the aggregate interlock mechanism to total shear resistance, which leads to more rapid deterioration under cyclic loading. Further research is needed to ensure the safety of using low coarse aggregate content in SCC in highly seismic areas and assess the safety of already existing buildings cast using SCC.

1. INTRODUCTION

Self-consolidating concrete (SCC) is a relatively recent development in concrete technology; its inception was in Japan in the late 1980s.[1] It has, however, been predicted that within the next decade, SCC would replace a significant portion of normal concrete (NC),[2,3] especially in developed countries. SCC has been generating significant interest and is gaining wider use in various projects worldwide. Its advantages over conventionally vibrated NC include: reduced labour; less noise and equipment on construction sites; and faster placement. Moreover, SCC ensures improved finish, hence reducing surface remedial costs and minimising wear and tear on formwork. It is a highly flowable yet stable concrete that can easily flow and consolidate, even in congested sections or complicated formwork, with little or no vibration and without undergoing significant segregation or bleeding.

SCC is usually produced using readily available conventional concrete materials. Its mixture proportions are based on creating high flowability while maintaining a relatively low water/cementitious materials ratio. This can be achieved through the use of high-range water reducing admixtures (HRWR) often in conjunction with rheology-modifying admixtures to ensure the stability and homogeneity of the mixture. The coarse aggregate content and its particle size gradation must be carefully controlled to enhance the flow of SCC, prevent blocking in densely reinforced sections and avoid segregation problems. The effects of the reduced coarse aggregate content, often used in formulating SCC, on its structural behaviour remain, however, largely unexplored.

A considerable portion of research performed on SCC was dedicated to its mixture proportions and rheological properties, while only a few studies focused on its structural applications. For instance, Nagai *et al.*[4] performed a research on the use of super-workable concrete in thin-walled prestressed precast concrete members. Their study showed an exceptional capacity of SCC to fill voids in heavily reinforced sections as thin as 60 mm with no significant segregation and no deleterious effects on durability. Research was also conducted on the compatibility of SCC with NC in sandwiched construction in order to reduce cost.[5] It was found that when casting structural members with SCC in congested areas and NC elsewhere in a sandwiched manner, such hybrid members behave satisfactorily.

Very limited studies were concerned with the structural performance of SCC in congested members compared with that of NC[6,7] and no study dedicated to the seismic performance of SCC was accessible in the open literature. Persson[3] performed a comparative study on NC and SCC to conclude that, for similar concrete strength, both concrete types behave similarly in terms of modulus of elasticity, creep and shrinkage. The relatively lower coarse aggregate content in SCC may, however, result in lower contribution to the shear resistance produced by aggregate interlock. The study performed by Schiessl and Zilch[9] confirmed such a behaviour through a monotonic test. Using roughness measurements, they found that crack surfaces of SCC were smoother than those of NC and that at a similar normal stress across the crack, SCC specimens exhibited lower

shear stress resistance. Studies on the shear strength of high-strength concrete have yielded similar conclusions. The improvement in concrete strength was achieved through enhancement of the transition zone between aggregates and cement paste. Thus, microcracks tend to propagate through aggregates rather than around them, and fracture surfaces become therefore smoother than those in NS concrete.[10] Accordingly, the shear capacity of SCC could be a concern, especially in the case of seismic loading.

For instance, moment-resisting frames (MRFs) are usually congested areas of reinforcement in which casting and consolidating concrete represents a substantial challenge. Such frames would be among the applications most benefiting from SCC since this material needs little or no vibration to be consolidated. The nature of reversed cyclic loading of MRFs in the event of an earthquake and the resulting plastic hinging would, however, impose cautiousness when SCC is used in such applications. Although SCC has been used in several buildings such as the Millennium Point Building in Birmingham, UK[1] without reported problems, investigations on the behaviour of SCC under cyclic loading are needed to ensure that a wide implementation of this material in earthquake-resistant structures is safe.

Several recent earthquakes demonstrated that beam–column joints are vital elements in keeping structural integrity. Fig. 1[11] shows a close-up of a non-ductile failure of a beam–column joint owing to the Kocaeli earthquake and illustrates that adequate performance of such joints during earthquakes is key for ensuring structural safety.

In the present paper, the behaviour of SCC beam–column joints under reversed cyclic loading is investigated and compared with that of NC beam–column joints in terms of load–displacement envelope, cumulative dissipated energy, steel and concrete contributions to beam and joint shear resistance and secant stiffness and the use of SCC in structural frames is discussed.

2. EXPERIMENTAL PROGRAMME

Beam–column joints can be isolated from plane frames at the points of contraflexure. The beam of the current test unit is taken to the mid-span of the bay, while the column is taken from the mid-height of one storey to the mid-height of the next storey. Two standard beam–column joints (J1 and J3) were designed as per the current CSA A23·3-94[12,13] requirements with adequate shear reinforcement in the joint area and in the hinging areas of the column and beam. The column is 3000 mm high with cross-section dimensions of 250 × 400 mm. The beam's length was 1750 mm from the face of the column to its free end with a cross-section of 250 × 400 mm. The longitudinal reinforcement used in the column was 14 M15 bars corresponding to a 2·8% reinforcement ratio (M15 is equivalent to a 16·0 mm diameter bar). The transverse reinforcement in the column was two M10 closed rectangular ties (M10 is equivalent to a 10·0 mm diameter bar).

Fig. 1. Beam–column joint failure in the Kocaeli 1999 earthquake (O'Rourke,[11] with permission)

The column ties are spaced at 80 mm inside the joint and for 500 mm above and below it (one-sixth of the floor's height) and then spaced at 125 mm for the rest of the column's height. The top and bottom longitudinal reinforcements of the beam are six M15 bars each corresponding to a 1·2% reinforcement ratio. The transverse reinforcement of the beam is M10 rectangular ties starting at 50 mm from the face of the column. The ties were spaced at 80 mm for the 800 mm adjacent to the column (equivalent to twice the beam's depth) and then spaced at 120 mm for the remaining 840 mm ending at 60 mm from the free end of the beam. The longitudinal rebar size and transverse reinforcement for the joint and hinging zones confinement satisfy current code requirements.

Reinforcement details for the tested specimens are shown in Fig. 2. NC and SCC were used to cast specimens J1 and J3, respectively. The concrete mixture proportions for both specimens are shown in Table 1. No vibration was used for casting the SCC specimen. Upon the release of the formwork, it was clear that the specimen constructed with SCC had less surface irregularities in comparison with the one made with NC. Fig. 3 illustrates exposed steel reinforcement which took place at several locations of specimen J1 despite the use of vibration. Specimen J3 cast without vibration did not exhibit such features.

2.1. Test set-up and procedure

The beam–column joint specimens were tested under a constant axial load of 600 kN applied on the column and reversed quasi-static cyclic loading applied at the beam tip. The selected loading pattern is intended to cause forces that simulate high levels of inelastic deformations that may be experienced by the frame during a severe earthquake. The selected load history consisted of two phases. The first phase was load-controlled followed by a displacement-controlled loading phase as shown in Fig. 4.

In the first phase of loading, two load cycles at approximately 10% of the estimated strength of the specimen were applied to check the test set-up and ensure that all data acquisition channels were functioning properly. This was followed by two load cycles reaching the concrete flexural cracking load in the beam at the column face. These in turn were followed by two cycles at the load causing initial yield in the beam measured through the load–displacement trace on the data acquisition monitor. The displacement at initial yield of the beam section at the column face, δ_y, was recorded and used in the subsequent displacement-controlled phase of loading.

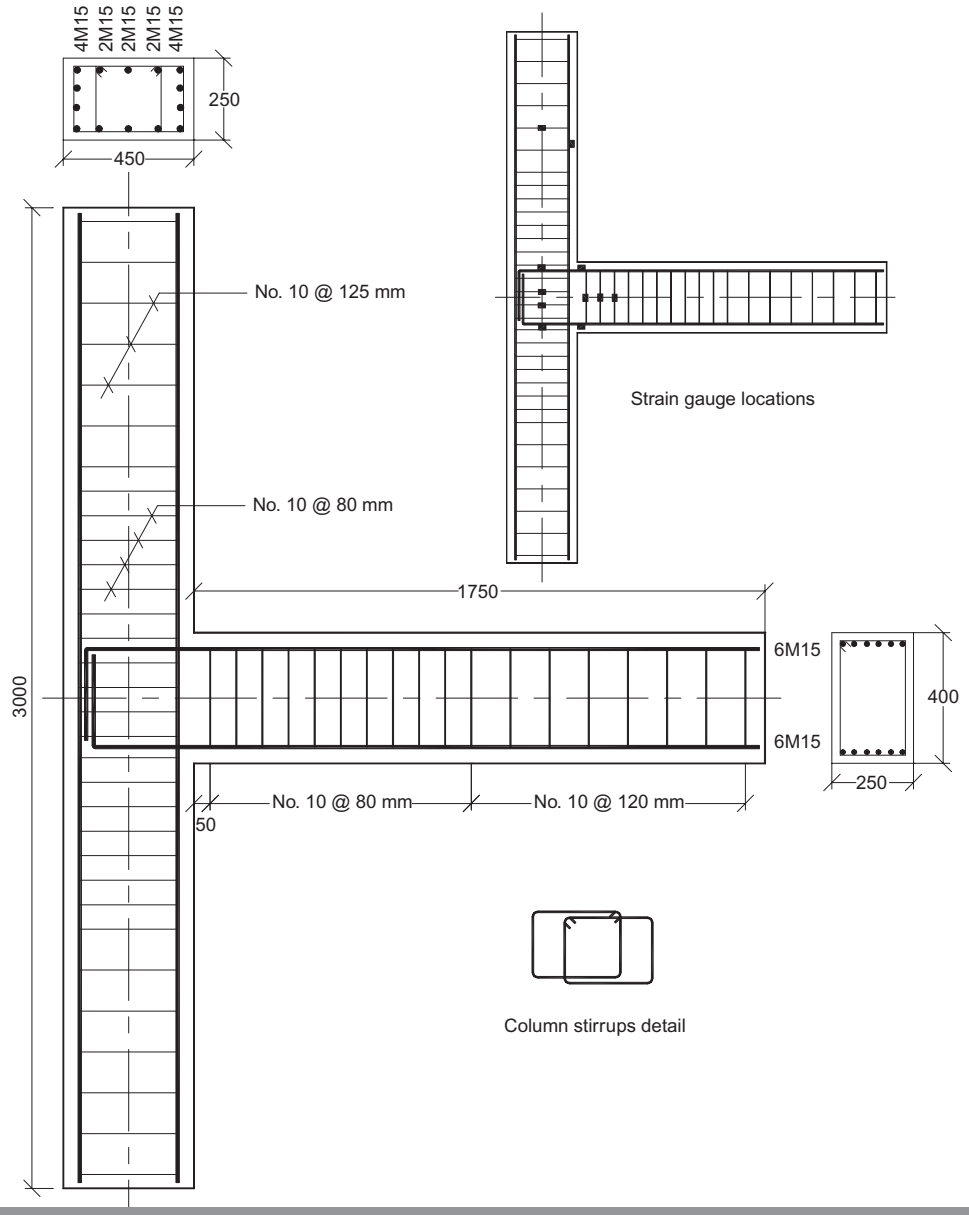

Fig. 2. Reinforcement details for the tested specimens (dimensions in mm)

	NC – J1	SCC – J3
Cement: kg/m^3	330	400
Sand: kg/m^3	790	850
Gravel: kg/m^3	1130	850
W/C	0·34	0·40
HRWR: l/m^3	—	4·0
WRA: ml/m^3	6·6	—
VMA: g/m^3	—	120
7 df'_c: MPa	37·2	33·3
28 df'_c: MPa	50·9	50·4
Slump: mm	50	—
Slump flow: mm	—	600

Table 1. Concrete mixture proportions for the tested specimens

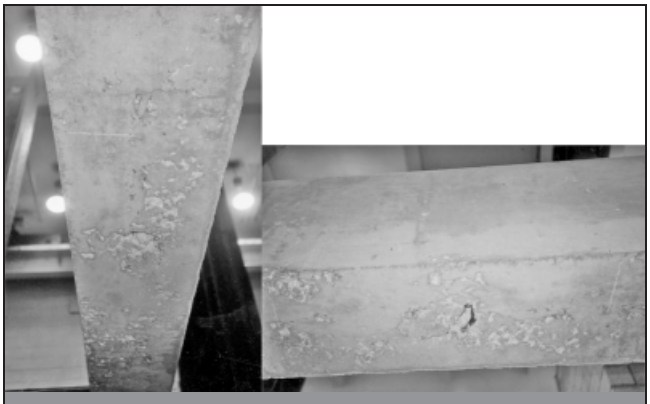

Fig. 3. Surface irregularities in NC specimen (J1)

The second phase of loading after first steel yield was displacement-controlled and consisted of applying the yield displacement for a second time then subsequently adding incremental multiples of the yield displacement δ_y (previously recorded at initial yield). Two load cycles were applied at each ductility level to verify the stability of the specimen. The ductility level is expressed in terms of a ductility factor, μ, which is defined as the ratio of the beam tip displacement, δ, to the displacement at first yield of the principal steel

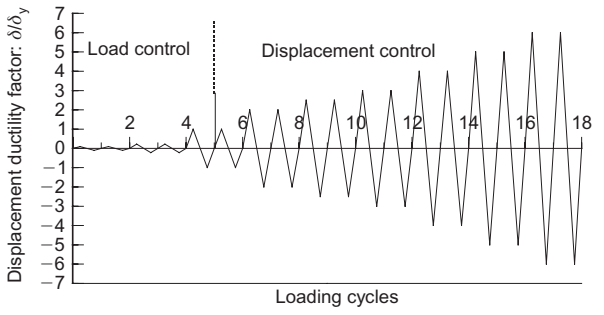

Fig. 4. Load history for the reversed cyclic load test used in the present study

reinforcement, δ_y. The test was stopped when the load-carrying capacity of the subassemblage dropped to about 50% of its maximum value. The effect of cyclic loading on the load-carrying capacity, strength degradation, energy dissipation and joint deformation was examined.

The effect of cyclic loading on the load-carrying capacity, energy dissipation, concrete contribution to shear resistance in the beam and the joint as well as strength degradation were examined.

The specimens were placed in the test rig as shown in Fig. 5 to mimic a hinge support at the base of the column and a roller support at the top part of the column. The roller support was created using a 2 cm vertical slot, which allowed vertical deformation in the column as well as the transmission of the column's axial load from the hydraulic jack to the lower hinge support. The cyclic load was applied at the beam tip using a loading ram through a greased pin connection located at 1670 mm from the column face. A view and a schematic of the test set-up are shown in Figs 5 and 6, respectively.

2.2. Instrumentation and data acquisition

Data from different monitoring devices were separated into analogue (load cells, displacement transducers) and digital (strain gauges) channels connected to the data acquisition unit, which was attached to a portable computer to record readings at a constant time interval of 5 s. The measured loads were the column's axial load and the beam's tip load. Two load cells were used for this purpose. Five linear variable displacement transducers (LVDTs) were used to measure the displacement at various locations on the specimen as shown in Fig. 6. One principal LVDT measured the beam's tip displacement and was fixed to an independent frame. Two half-inch LVDTs were used in the joint area to measure the joint's distortion. These LVDTs were fixed to previously installed bolts in the joint panel of the specimen. Two other one-inch LVDTs were fixed on the top and bottom of the beam to measure the slippage of bars in it. Small aluminium plates were fixed for these LVDTs stems to butt against.

Strains in the reinforcing steel were monitored using electrical resistance strain gauges, which were fixed to the deformed bars after being ground to expose straight clean flat surface. The wiring was bundled to come out of the concrete at specific spots. The location of strain gauges on the longitudinal and

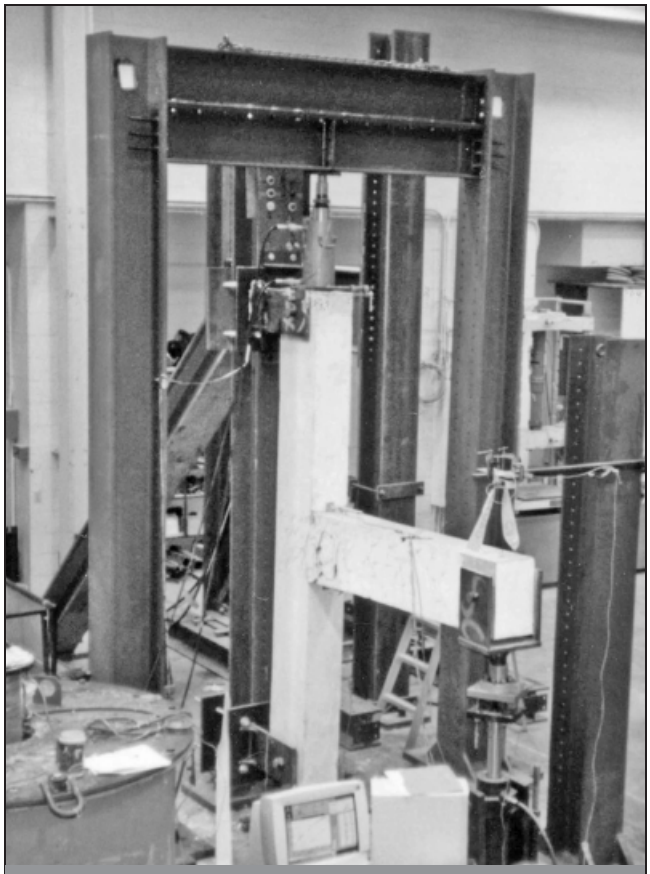

Fig. 5. View of the test rig

transverse reinforcement bars in the beam and column are shown in Fig. 2.

3. RESULTS AND DISCUSSION

3.1. Behaviour of specimens

The load–storey drift plots for the NC (J1) and SCC (J3) specimens are shown in Figs 7 and 8, respectively. First flexural cracking of the beam section subjected to maximum bending moment appeared at a beam tip load of 15 and 17 kN corresponding to a drift of 0·17% and 0·18% for specimens J1 and J3, respectively. The onset of diagonal cracks in the joint area took place at a beam tip load of 60 and 65 kN corresponding to a drift of 0·6% and 0·5% for specimens J1 and J3, respectively. Additional cracks appeared thereafter as loading progressed at a uniform spacing, but remained within a very fine width throughout the test.

For the NC specimen, the yield of the beam's longitudinal steel was reached at an average beam tip load of 107 kN and the corresponding average yield displacement was 28 mm (corresponding to a drift of 1·5%, based on push up and pull down values), whereas for the SCC specimen, the yield load was 104 kN at a displacement of 27 mm (corresponding to a drift of 1·4%).

At a ductility factor of 2 (corresponding to a drift of 3·0%), both specimens developed extensive cracking in the beam along a distance equal to its depth from the face of the column. At a ductility factor of 3 (corresponding to a drift of 4·5%), the SCC specimen started exhibiting lower load-carrying capacity

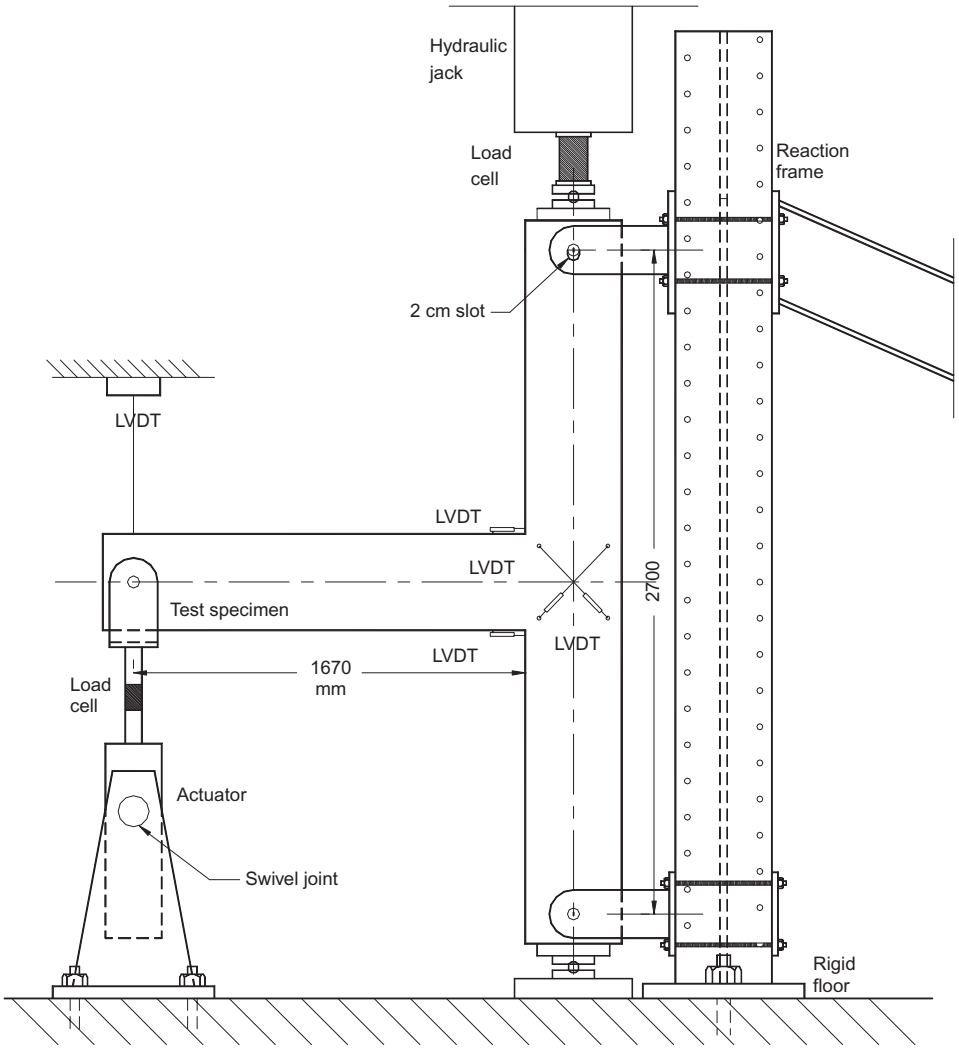

Fig. 6. Test set-up

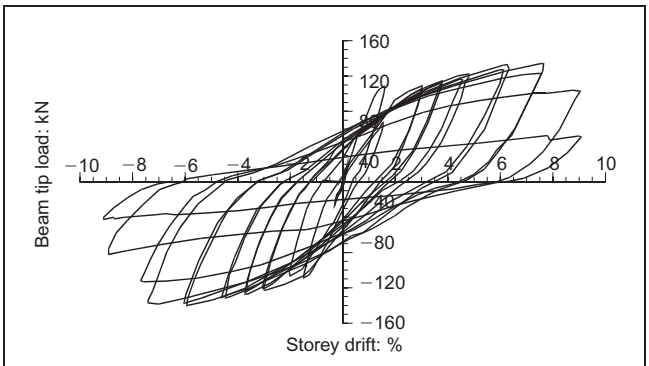

Fig. 7. Load–storey drift relationship for NC specimen J1

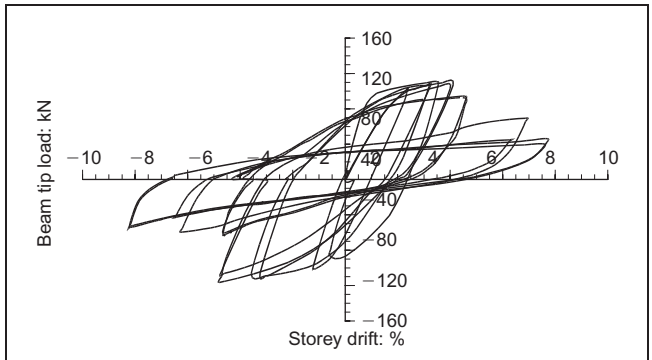

Fig. 8. Load–storey drift relationship for SCC specimen J3

compared with that of the NC specimen. This became even clearer in subsequent load cycles. For both specimens the column's axial load was maintained and the joint areas were still intact, except the presence of fine diagonal cracks. The faster decline of the load-carrying capacity of the SCC specimen could be attributed to the fact that its lower coarse aggregate reduced the contribution of friction due to aggregate interlock to the total shear resistance mechanisms, especially at high levels of displacement. Final crack patterns for the NC (J1) and the SCC (J3) beam–column joint specimens are shown in Figs 9 and 10, respectively.

3.2. Load–storey drift envelope relationship

For each of the beam–column joint specimens, the envelope of the beam tip load–displacement relationship is plotted in Fig. 11. The SCC specimen (J3) had a comparable capacity to that of

the NC (J1) specimen up to a displacement level of about 75 mm (corresponding to a 4·5% drift), which could be considered as structurally adequate. Subsequently, the reserve strength of the SCC specimen was lower and a plastic hinge formed in the beam. The maximum displacement ductility achieved by the NC specimen was 6 compared with 5 for the SCC specimen.

Fig. 9. Final crack pattern for NC specimen J1

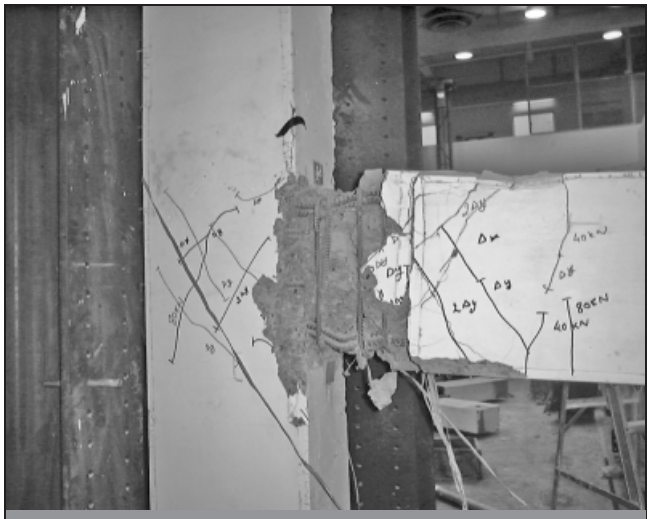

Fig. 10. Final crack pattern for SCC specimen J3

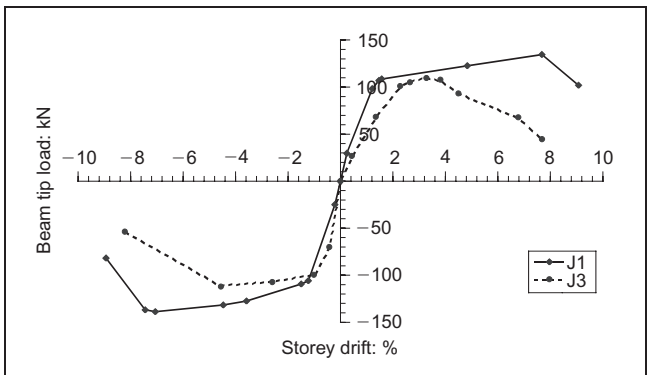

Fig. 11. Load–storey drift envelopes for the NC and SCC specimens

3.3. Cumulative dissipated energy

The capability of a structure to survive an earthquake depends on its ability to dissipate the energy input from ground motion. Despite the fact that energy input during a ground movement event is difficult to estimate, a satisfactory design should ensure a larger energy dissipation capability of the structure than the demand. The cumulative energy dissipated by the beam–column joint specimens during the reversed cyclic load tests was calculated by summing up the energy dissipated in consecutive load–displacement loops throughout the test. The energy dissipated in a cycle is calculated as the area that the hysteretic loop encloses in the corresponding beam tip load–displacement plot.

Figure 12 shows a plot of the cumulative energy dissipation versus the storey drift for the NC specimen (J1) and the SCC specimen (J3). Results show that the SCC joint had higher energy dissipation up to a ductility level of 3 corresponding to about 6% storey drift. Afterwards, the NC joint specimen showed higher energy dissipation capacity with an overall 38% superiority.

3.4. Shear in beams

The shear force applied to the beam section is resisted by the steel and concrete. Ever since Ritter[14] followed by Mörsch[15] formulated the truss analogy approach, several methods emerged to calculate the shear capacity of reinforced concrete (RC) beams based on their approach. Analytical methods in the literature such as the modified compression field theory[16] can more precisely estimate the shear capacity of RC beams and calculate the individual contribution of concrete and steel to shear strength. Despite their scientific appeal, however, such methods still remain complicated and involve intensive calculations. Accordingly, the 45° truss analogy approach remains quite widely adopted.

Typically, the shear capacity of the beam is assumed to be simultaneously supplied by concrete and the transverse steel reinforcement according to the expression:

$$V_t = V_c + V_s \quad (1)$$

where, V_t is the total shear force in the beam, V_c is the shear force resisted by concrete and V_s is the shear force resisted by the transverse steel reinforcement. Adopting the 45° truss

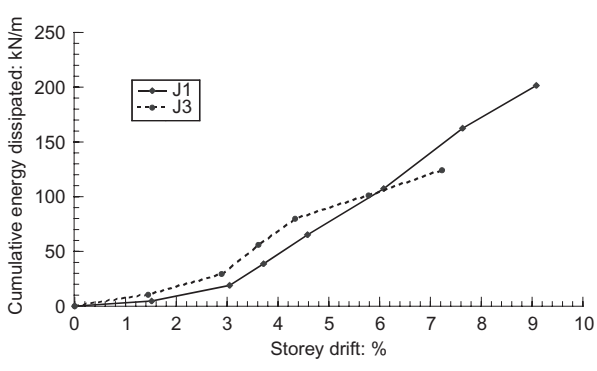

Fig. 12. Cumulative energy dissipated for the NC and SCC specimens

analogy, the shear resistance provided by the transverse reinforcement can be expressed as:

$$V_s = \frac{A_v f_s d}{s} \quad (2)$$

where s is the spacing of transverse steel reinforcement, A_v is the area of transverse reinforcement over a distance s, f_s is the stress in the transverse reinforcement and d is the distance from the extreme compression fibre to tension reinforcement.

The strains measured in the stirrups were converted into stresses then used to evaluate the shear resistance of the transverse reinforcement according to equation (2). The stress in the steel, f_s, was based on the average strain obtained from three strain gauge measurements mounted on the first three stirrups in the beam from the column face.

The Canadian Standard Association concrete design provisions[12] evaluate the concrete shear strength, V_c, for nominal ductility members as

$$V_c = 0{\cdot}2\sqrt{f'_c}\, b_w d \quad (3)$$

where f'_c is the compressive strength of concrete cylinder, b_w is the beam's breadth and d is the effective beam's depth. Figs 13 and 14 illustrate the individual contribution of concrete and steel to the shear resisted by concrete and transverse steel reinforcement for specimens J1 and J3, respectively. Fig. 13 shows that for specimen J1, the maximum concrete contribution to the beam shear occurred at a ductility level of 2 (corresponding to a drift of 3·0%) with a value of 110 kN (corresponding to $0{\cdot}18\sqrt{f'_c}\, b_w d$). At a displacement ductility factor of 6 (corresponding to a drift of 9·0%), the concrete was still resisting some of the beam shear load with a value of 26 kN (corresponding to $0{\cdot}05\sqrt{f'_c}\, b_w d$). Fig. 14 shows that for specimen J3 the maximum concrete contribution to the beam shear resistance occurred at displacement ductility of 2·0 (corresponding to a drift of 2·8%) with a value of 98 kN (corresponding to $0{\cdot}16\sqrt{f'_c}\, b_w d$). At a displacement ductility of 5·0, the contribution of concrete was minor and the transverse reinforcement resisted almost all the shear load. An examination of Figs 13 and 14 reveals that the concrete in the

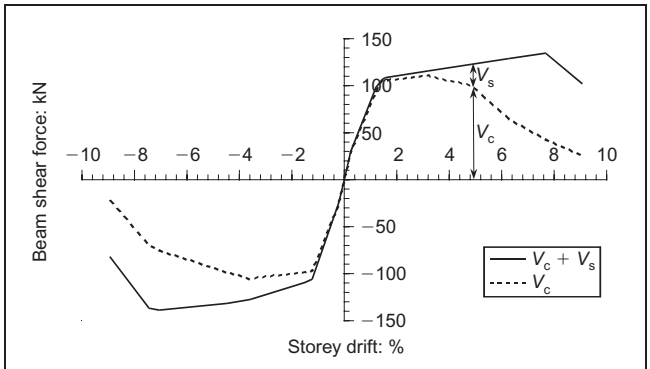

Fig. 13. Beam shear force resisted by concrete and transverse steel reinforcement plotted against storey drift envelopes for the NC specimen J1

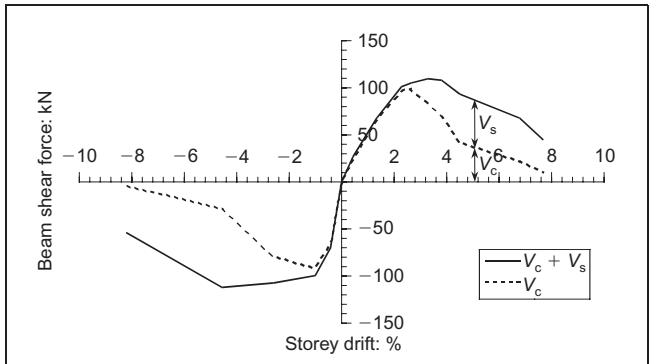

Fig. 14. Beam shear force resisted by concrete and transverse steel reinforcement plotted against storey drift envelopes for the SCC specimen J3

NC specimen carried a higher percentage and magnitude of the shear force applied on the beam compared with that in the SCC specimen. Fig. 15, which shows the beam-tip load plotted against strain in the second stirrup in the beam from the face of the column, indicates higher levels of strain in the stirrups of specimen J3 compared with that in specimen J1 at corresponding loading levels. An analogy to the case of the smooth crack surface in SCC is high-strength concrete (HSC). A study performed by Walraven[17] indicated that the shear friction in HSC beams is up to 35% lower than that in NSC beams. This is attributed to the fact that the shear fracture surface in HSC members is usually transgranular (propagates across coarse aggregates) and is therefore smoother than that in NSC members.[11] It is worth noting that the beams' plastic hinges formed at equal distances from the column face for both specimens.

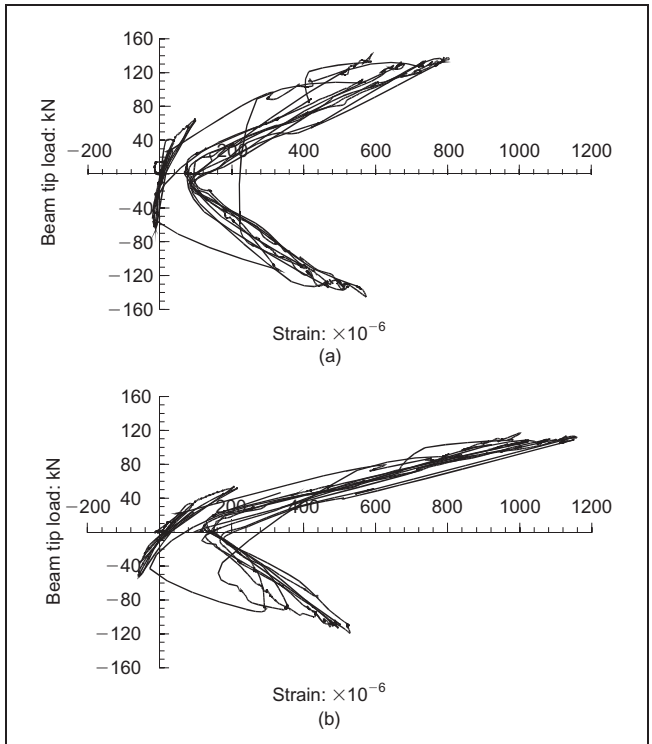

Fig. 15. Beam tip load plotted against second steel stirrup strain for specimen: (a) J1 and (b) J3

3.5. Joint behaviour

The shear force input to the joint from the beam is expressed as

$$V_{jt} = A_s\ f_s - V_{col} \quad (4)$$

where V_{jt} is the total joint shear force, A_s is the cross-sectional area of the tensile reinforcement in the beam, f_s is the stress in the longitudinal tensile reinforcement in the beam, and V_{col} is the column shear force that can be obtained by static equilibrium of the subassemblage (Fig. 16(b)) as follows

$$V_{col} = \frac{P\ (L/2)}{H} \quad (5)$$

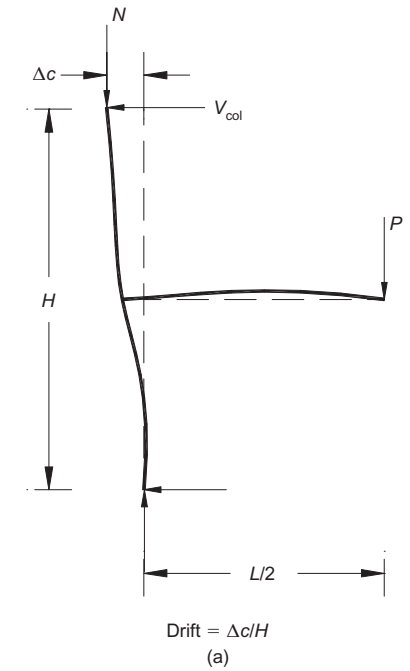

Fig. 16. Exterior beam–column subassemblages in (a) displaced frame and (b) test rig

The joint shear is resisted by both the concrete and the transverse reinforcement. The shear force resisted by the transverse reinforcement can be calculated as

$$V_{js} = A_v\ f_{st} \quad (6)$$

where A_v is the total area of the transverse reinforcement in the joint, and f_{st} is the stress in the joint transverse reinforcement calculated using the averaged strains measured by the strain gauges on stirrups in the joint.

The joint shear is plotted against storey drift for tested specimens and is presented in Figs 17 and 18. Strain gauge readings revealed that the first values of strain were recorded at the onset of cracks in the joint area for both specimens. The results given in Fig. 17 for specimen J1 show that concrete carried the majority of joint shear up to approximately 1·5% drift, corresponding to the yielding of steel in the beam section. As the test progressed, the contribution of steel slightly increased, but the concrete contribution remained significant. Fig. 18 similarly shows that concrete was the major contributor to joint shear resistance. As the test progressed, the beam capacity declined resulting in a decrease in joint shear.

It was noted that the steel contribution to shear resistance was lower in the joint panel area than that at the beam hinging area. This is mainly attributed to the extent of cracking and the

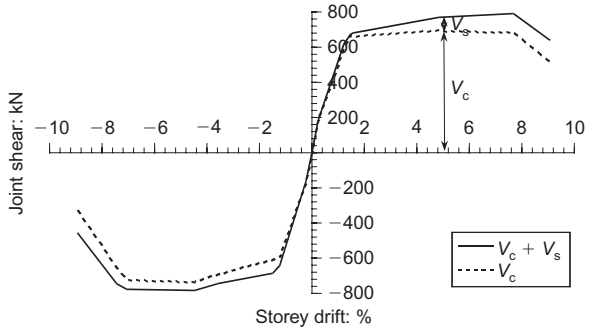

Fig. 17. Joint shear force resisted by concrete and transverse steel reinforcement plotted against storey drift envelopes for the NC specimen J1

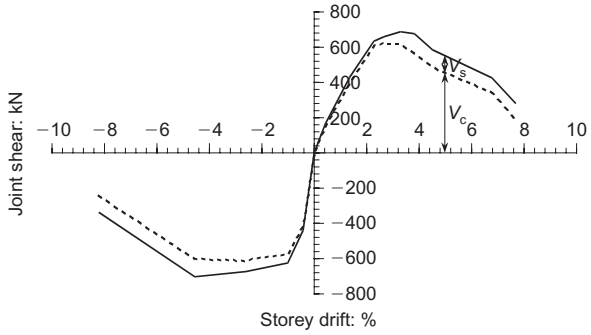

Fig. 18. Joint shear force resisted by concrete and transverse steel reinforcement plotted against storey drift envelopes for the SCC specimen J3

associated slippage along the cracks, which is significantly higher in the case of the hinging zone of the beam than that in the slightly cracked joint panel. It is worth mentioning that for both specimens, at the same levels of joint shear input, the calculated joint deformations were comparable.

3.6. Secant stiffness

Secant stiffness is evaluated as the peak-to-peak stiffness of the beam tip load–displacement relationship. It is calculated as the slope of the line joining the peak of positive and negative loads at each given cycle. The secant stiffness is an index of the response of the specimen during a cycle and its strength degradation from one cycle to the following cycle.

Figure 19 shows plots of the secant stiffness for the NC and SCC beam–column joint specimens plotted against the storey drift. The storey drift is calculated as shown in Fig. 16 by relating the subassemblage deformation in the test rig to the actual displaced frame case. An examination of the plots indicates that the SCC specimen (J3) had higher initial stiffness. After a drift angle of 2%, the NC standard specimen (J1) had higher stiffness up to the end of the test. Nonetheless, the SCC specimen (J3) exhibited stable strength degradation up to failure. The maximum drift achieved was 9·0% and 7·9% for specimens J1 and J3, respectively.

4. CONCLUSIONS

Reversed cyclic loading tests were performed on full-scale beam–column joint specimens to compare the performance of NC and SCC in moment-resisting frames. Based on experimental observations and analysis of test results, the following conclusions can be drawn.

1. SCC beam–column joints have comparable load capacity to that of NC joints up to a certain ductility level. At high ductility levels, SCC specimens may not maintain the same load-carrying capacity as NC specimens. While this could be attributed to the fact that the lower coarse aggregate content in SCC reduced the contribution of the aggregate interlock to the total shear resistance mechanism, further research is required fully to understand this behaviour.
2. The performance of SCC under shear stress in the joint panel was comparable to that of NC in terms of cracking and deformations.

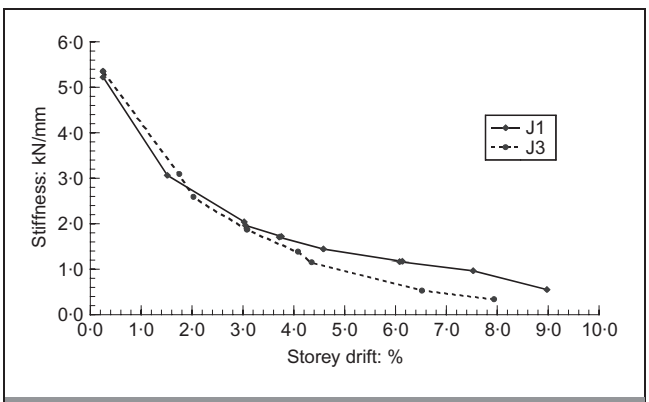

Fig. 19. Secant stiffness–storey drift for the NC and SCC specimens

3. The SCC beam–column joint specimen performed adequately in terms of the mode of failure and ductility requirements, assuming that the expected minimum drift requirement is 3%, as recommended in the literature for ductile frame buildings.[18]
4. The contribution of concrete to the shear resistance in the beam of the NC beam–column specimen was higher than that of the SCC specimen, especially at high drifts. In the case of the joint, the concrete contribution to shear resistance remained significant until the end of the test for both specimens. The difference in both cases was attributed to the smaller slippage along cracks in the joint area compared with that in the beam hinging zone.
5. Further studies are needed to investigate the behaviour of SCC under cyclic loading in hinging zones and to quantify aggregate interlock contribution mechanisms for different coarse aggregate contents and maximum aggregate size along with the effect of other mixture design parameters.

ACKNOWLEDGEMENTS

The continuous support of the Natural Science and Engineering Research Council of Canada (NSERC), the Ontario Centres of Excellence (OCE), the Canada Foundation for Innovation (CFI) and the Ontario Innovation Trust (OIT) to the research programmes of Professor Moncef Nehdi has been essential for the development of this research.

REFERENCES

1. NAGAMOTO N. and OZAWA K. Mixture properties of self-compacting, high-performance concrete. *Proceedings of the Third CANMET/ACI International Conference on Design and Materials and Recent Advances in Concrete Technology*, ACI SP 172, Kuala Lumpur, Malaysia, 1997, pp. 627–637.
2. CAMPION M. J. and JOST P. Self-compacting concrete—expanding the possibilities of concrete design and placement. *Concrete International*, 2000, **22**, No. 4, 31–34.
3. HENDERSON N. Self compacting concrete at millennium point. In *Concrete for the Construction Industry*, The Concrete Society, UK, 2000, pp. 26–27.
4. NAGAI T., KOJIMA T. and MIURA T. Application of high strength/superworkable concrete to thin-wall prestressed concrete products. *Magazine of Concrete Research*, **51**, No. 3, 153–162.
5. HO D. W. S., SHEINN A. M. M. and TAM C. T. The sandwich concept of construction with SCC. *Cement and Concrete Research*, 2001, **31**, No. 9, 1377–1381.
6. KHAYAT K. H., PAULTRE P. and TREMBLAY S. Structural performance and in-place properties of self-consolidating concrete used for casting highly reinforced columns. *ACI Materials Journal*, 2001, **98**, No. 5, 371–378.
7. SONEBI M., BARTOS P. and TAMIMI A. Flexural response of reinforced beams cast with self-compacting concrete. *Proceedings of the Second International Symposium on Self-Compacting Concrete*, Tokyo, Japan, RILEM Publications S.A.R.L., 2001, pp. 517–526.
8. PERSSON B. A comparison between mechanical properties of self-compacting concrete and the corresponding properties of normal concrete. *Cement and Concrete Research*, 2001, **31**, No. 2, 193–198.
9. SCHIESSL A. and ZILCH K. The effect of the modified composition of SCC on shear and bond behaviour.

Proceedings of the Second International Symposium on Self-Compacting Concrete, Tokyo, Japan, RILEM Publications S.A.R.L., 2001, pp. 501–506.
10. EL CHABIB H., NEHDI M. and SAID A. Predicting shear capacity of NSC and HSC slender beams without stirrups using artificial intelligence. *Computers and Concrete,* 2005, **2**, No. 1, 79–96.
11. O'ROURKE T. D. *The Turkey, Taiwan, and Mexico City Earthquakes: Lessons Learned*. Hearing of the Subcommittee on Basic Research U.S. House of Representatives Committee on Science, October 20, 1999. See http://mceer.buffalo.edu/outreach/Congress/TRtestimony.asp
12. CANADIAN STANDARDS ASSOCIATION. *Design of Concrete Structures. CSA A23·3-94*. CSA, Rexdale, Ontario, Canada, 1994, 209 p.
13. AMERICAN CONCRETE INSTITUTE/AMERICAN SOCIETY OF CIVIL ENGINEERS. *Recommendations for Design of Beam-Column Connections in Monolithic Reinforced Concrete Structures*. Joint ACI/ASCE Committee 352, Technical Committee Document 352R-02, 37pp.
14. RITTER W. Die Bauweise Hennebique. *Schweizerische Bauzeitung*, 1899, **33**, No. **7**, 59–61.
15. MÖRSCH E. *Concrete Steel Construction*, 3rd edn (1st edn in 1902). Engineering News Publishing Co, New York, 1909, 368 p. Translated into English by E. P. Goodrich of Der Eisenbetonau.
16. VECCHIO F. J. and COLLINS M. P. The modified compression field theory for reinforced concrete elements subjected to shear. *ACI Journal Proceedings*, 1986, **83**, No. 2, 219–231.
17. WALRAVEN J. C. Shear friction in high strength concrete. *Progress in Concrete Research*, Delft University of Technology, The Netherlands, 1995, Vol. 4, pp. 57–65.
18. CORLEY W. G. Ductility of columns, walls, and beams—how much is enough? *Proceedings of the Thomas Paulay Symposium on Recent Developments in Lateral Force Transfer in Buildings*, ACI SP-157, La Jolla, California, 1995, pp. 331–350.